SPACE ROBOTS

Exploring planet geology through force-feedback telemanipulation from orbit

Copyright © 2022 The Authors, some rights reserved; exclusive licensee American Association for the Advancement of Science. No claim to original U.S. Government Works

Michael Panzirsch[1]*†, Aaron Pereira[1,2]†, Harsimran Singh[1]*†, Bernhard Weber[1], Edmundo Ferreira[2], Andrei Gherghescu[2], Lukas Hann[2], Emiel den Exter[2], Frank van der Hulst[2,3], Levin Gerdes[2,4], Leonardo Cencetti[2,5], Kjetil Wormnes[2], Jessica Grenouilleau[2], William Carey[2], Ribin Balachandran[1], Thomas Hulin[1], Christian Ott[1], Daniel Leidner[1], Alin Albu-Schäffer[1], Neal Y. Lii[1]‡, Thomas Krüger[2]‡

Current space exploration roadmaps envision exploring the surface geology of celestial bodies with robots for both scientific research and in situ resource utilization. In such unstructured, poorly lit, complex, and remote environments, automation is not always possible, and some tasks, such as geological sampling, require direct teleoperation aided by force-feedback (FF). The operator would be on an orbiting spacecraft, and poor bandwidth, high latency, and packet loss from orbit to ground mean that safe, stable, and transparent interaction is a substantial technical challenge. For this scenario, a control method was developed that ensures stability at high delay without reduction in speed or loss of positioning accuracy. At the same time, a new level of safety is achieved not only through FF itself but also through an intrinsic property of the approach preventing hard impacts. On the basis of this method, a tele-exploration scenario was simulated in the Analog-1 experiment with an astronaut on the International Space Station (ISS) using a 6–degree-of-freedom (DoF) FF capable haptic input device to control a mobile robot with manipulator on Earth to collect rock samples. The 6-DoF FF telemanipulation from space was performed at a round-trip communication delay constantly between 770 and 850 milliseconds and an average packet loss of 1.27%. This experiment showcases the feasibility of a complete space exploration scenario via haptic telemanipulation under spaceflight conditions. The results underline the benefits of this control method for safe and accurate interactions and of haptic feedback in general.

INTRODUCTION

High-fidelity haptic interaction in planetary sampling

Space exploration—one of the most challenging technical endeavors of this age—is driven by human curiosity and the pursuit of knowledge. Besides scientific ambitions, industrial interests, including mining rare resources on celestial bodies, play an increasingly prominent role. Because bringing humans to the surface of the moon or other celestial bodies is dangerous and costly, many tasks—such as exploration, investigation of regolith and geology, and sample collection—can be performed by robots.

Two of the first robotic arms on celestial body surfaces were used for sample collection in the Lunar 16 mission of the Soviet Luna program in 1970 and on Mars in 1975 in the NASA Viking mission. The first rover equipped with a robotic arm was launched in 2003 to Mars (*1*). In the recent past, robotic arms of varying complexity were also sent to comets and asteroids in the European Space Agency (ESA) Rosetta (*2*, *3*) and the NASA OSIRIS-REx missions (*4*), respectively. Upcoming missions aim also for the Martian moon Phobos. For instance, the MMX rover (*5*) equipped with a robotic arm is planned to reach Mars orbit in 2025. These past missions and future plans of major space agencies focus on the collection, and in situ analysis or return, of geological samples.

[1]German Aerospace Center (DLR), Robotics and Mechatronics Center, Wessling, Germany. [2]European Space Agency (ESA), Noordwijk, Netherlands. [3]MF Robotics, Leiden, Netherlands. [4]Department of Systems Engineering and Automation, University of Málaga, Málaga, Spain. [5]École polytechnique fédérale de Lausanne (EPFL), Lausanne, Switzerland.
*Corresponding author. Email: michael.panzirsch@dlr.de (M.P.); harsimran.singh@dlr.de (H.S.)
†These authors contributed equally to this work.
‡These authors equally shared the project lead.

Whereas tasks in structured environments, such as habitat building, may be performed by robots partially autonomously (*6*), explorative tasks such as sample collection take place in unknown, unstructured environments. Here, including human capabilities (e.g., perception and problem solving) into the control loop is indispensable. Even after advances in automation and artificial intelligence, an interface for direct control by a human will still be crucial in case of system failures or unexpected complications and for extending the robots' capabilities beyond those envisioned by the developers (*7*).

Limited bandwidth in space communications and poor lighting conditions impair video quality during teleoperation and hence the operator's feeling of immersion. Being able to feel interaction forces between the robot and its environment through the haptic interface can help restore this immersion. The perception of contacts with the rock samples also helps to operate safely and more precisely. Further, the operator can feel the weight of the rocks grasped or properties of the regolith such as cohesion, internal friction, and density. Thus, teleoperation presents an ideal combination of human capabilities with the dexterous precision and robustness of robotic systems. In several meta-analyses (*8*, *9*), it was shown that force-feedback (FF) significantly enhances teleoperation due to a more natural and intuitive interaction. Still, state-of-the-art control approaches for FF provide insufficient performance in terms of position tracking and safety in the targeted delay range.

Background and related work

Teleoperation of robots in space has a long history aboard space shuttles (*10*, *11*, *12*), on satellites (*13*, *14*), and on the International Space Station (ISS) (*15*).

Downloaded from https://www.science.org at The Hong Kong University of Science and Technology (Guangzhou) on May 25, 2026

Teleoperation in space applications

Early teleoperation systems used position-controlled robots, sometimes equipped with force-torque sensors at the end effector. In contrast to more recent experiments, these robots were not impedance controlled and therefore were incapable of safe, compliant interactions.

Also, because of the lack of adequate control approaches for delayed teleoperation with FF, early concepts were often based on predictive virtual displays and relied partially on autonomous capabilities of the robot. The first remotely controlled robot in space was in the ROTEX mission on the Space Shuttle orbiter Columbia (*12*), operated from ground at 7 s round-trip delay (RTD) with the help of predictive virtual displays, shared control, and motion primitives. Soon after, a robot was installed on the Japanese engineering test satellite ETS-VII and used for a variety of teleoperation experiments, including not only predictive virtual displays (*14*) but also FF to ground (*16*). Besides these robots dedicated to research, the Shuttle Remote Manipulator System (SRMS) (*10*, *11*) and, much later, the Space Station Remote Manipulator System (SSRMS) (*15*) and the Special Purpose Dexterous Manipulator (SPDM) were implemented on space shuttles and the ISS, respectively. These robots are meant for tasks such as docking maneuvers and for the positioning of external payloads using multiple cameras and manual control. Despite the complexity of applications, the control interface is based on a separate 3-DoF (degree of freedom) translational and a 3-DoF rotational hand controller for teleoperation without FF at zero delay. Later, a two-axis torque-controlled lightweight robot was installed outside the ISS in the ROKVISS experiment (*17*) to test robotic hardware and teleoperation from ground. This robot had torque sensing in each joint and paved the way for more modern torque-controlled space robots.

FF in teleoperation space experiments

FF, or force reflection, differs from predictive virtual FF approaches in that the force displayed on the input device is measured on the remote robot side and transmitted to the operator. This was first tested in ground-to-space setups. With advances in robotic hardware, robots could be teleoperated in impedance control. In (*17*), 2-DoF teleoperation of a two-joint impedance-controlled robot on the ISS via a joystick on ground was validated for S-band communication with approximately 30-ms RTD. In contrast, in (*16*), a position-position control architecture, in which the positions of robot and input device are exchanged through the communication channel, was applied to achieve a direct bilateral coupling in 2-DoF under 7-s RTD.

Later, the scenario was inverted to space-to-ground teleoperation, with astronauts on the ISS controlling robots on Earth. In the Interact mission (*18*), a sensitive 1-DoF peg-in-hole task was performed at about 850-ms RTD via a rover equipped with a robotic arm, after navigation of the rover and autonomous positioning of the robotic arm. In the inverted ROKVISS setup of the Kontur-2 mission *(19)*, a 2-DoF experiment was performed by cosmonauts on the ISS over S-band communication to evaluate effects of microgravity on the human operator's performance in tasks involving free motion and haptic interaction (*20*). It suggested that degraded sensorimotor performance persists even after adaptation and that FF provides a benefit both in microgravity and on Earth. Still, features such as damping, which help with accuracy under terrestrial conditions, can have a detrimental effect in microgravity.

Robotic tasks

Via direct bilateral coupling, the tasks performed have been mostly basic, such as peg in hole and slope tracing (*16*, *17*). Before our experiment, only one or two DoFs of a robot have been controlled with FF. The cooperative task between a cosmonaut on the ISS and a second operator on ground in the multilateral setup of (*21*) served as a concept analysis based on an abstract task with a limited number of DoFs. In a ground-to-ground experiment with approximately 600-ms RTD, direct telemanipulation was used to grasp and stabilize a client satellite by a servicer satellite. This showed the aptitude of modern control concepts for delayed bilateral coupling where high transparency in the display of the robot's environmental impedance is needed (*22*).

In early works (*12*, *23*), assembly, maintenance, and inspection tasks could be achieved in highly structured and known environments with the support of autonomous functionalities. Also, in a well-structured environment, the SUPVIS-JUSTIN experiments showcased more complex infrastructure setup and maintenance tasks (including unexpected scenarios) by a humanoid robot (*24*) controlled from the ISS via a tablet interface in supervised autonomy (*6*, *25*).

Control for FF telemanipulation

A large variety of stability approaches for delayed control have been proposed in the past decades, ranging from Lyapunov theory and frequency-based approaches, such as L2-stability and the Raisbeck or Llewellyn criteria, to the currently more prominent time domain–based approaches. For instance, the position-position control developed for telemanipulation at 7-s RTD (*16*) was stabilized on the basis of the Llewellyn criterion for absolute stability. Note that the position-position architecture itself already leads to a highly damped coupling behavior. In contrast to these frequency-based approaches, which require constant conservative controller parametrization, time domain–based approaches such as the time domain passivity approach (TDPA) *(26)* and the wave-variables concept *(27)* are adaptive over time and thus less conservative.

The latter was shown to result in overall lower performance in terms of position tracking and transmitted impedances than TDPA at high delay (*28*). Furthermore, TDPA is intrinsically robust to packet loss, jitter, and variable delay, which renders it highly appropriate for the space communication infrastructure. Therefore, TDPA was later applied in several space missions as the 1-DoF system of Haptics-1 (*29*), the 2-DoF system of Kontur-2 (*19*) with the cooperative scenario of (*21*), and the 6-DoF system of the ground-to-ground experiment (*22*). TDPA was extended to more complex bilateral coupling including measured forces in (*30*) and (*31*).

These previous works paved the way for Analog-1. Through the enhancement of the TDPA approach presented in this paper, a complete space exploration scenario from the ISS was now possible.

Contributions

This paper presents a control concept for safe, stable, and transparent space teleoperation and results of the 6-DoF closed-loop telemanipulation with FF from a spacecraft to ground. The communication was routed via geostationary satellites resulting in a round-trip communication delay of around 810 ± 40 ms and a packet loss of 1.27%.

Previous research showed degradation of human sensorimotor performance during motion and force application tasks in microgravity (*32*, *20*, *33*). Because of this and other unique conditions of space missions (e.g., high workload), a feasibility study must be conducted under real spaceflight conditions to derive reliable insights and should not simply be simulated in a terrestrial setup.

With large delays, stability must be ensured. However, previous control concepts for ensuring stability cannot sufficiently prevent

Downloaded from https://www.science.org at The Hong Kong University of Science and Technology (Guangzhou) on May 25, 2026

hard collisions, because the collision is sensed too late by the operator. They also suffer from position drift, where the velocity is attenuated in free motion. In addition, large delays decrease transparency of the teleoperation, because the reflected visual feedback and forces displayed on the haptic input device do not correspond immediately to the commanded motion. This may lead to unsafe motion.

To address the problem of hard collisions, a control concept for direct teleoperation was developed for the Analog-1 mission. Our approach reduces the position drift in free motion from 59% to below 1%, meaning that motions of the input device are well tracked by the robot, and ensures that high forces are only applied after the astronaut has perceived a contact and pressed against it.

The subjective ratings of the astronaut indicate a low level of overall workload and that the control is intuitive and provides a sufficiently natural feeling of interaction. This is supported by objective data that were gathered during a proficiency run and the final experiment and that show a fast training effect in terms of maximum forces, required time for execution, number of wrong grasps, and indexing. Indexing refers to the decoupling of input device and robot with subsequent repositioning of the input device, which is often used to extend its workspace.

The main contributions of the presented work can be summarized as follows: An astronaut on the ISS teleoperated a robot on Earth in 6-DoF with FF. The study validates the feasibility of 6-DoF teleoperation with FF via geostationary relay satellites and spaceflight conditions for the human operator. Previous control approaches to handle high delays struggled with continual high damping and position drift and did not limit forces on contact with the environment. This work presents an approach for safe and stable interactions at extreme delays while remaining transparent for the user. The case study considers workload, situational awareness, and sensorimotor performance of an astronaut operating under real spaceflight conditions and shows the feasibility of complex robot teleoperation from an orbiting spacecraft.

RESULTS

Experimental setup

The experiment was conducted in a lunar analog scenario prepared in Valkenburg, The Netherlands (*34*) (see Fig. 1A) 4 months into astronaut Luca Parmitano's stay on the ISS. There were three sampling sites (S1, S2, and S3), and the paths between them were marked with cones. At each site, the astronaut selected two rock samples in consultation with a team of geologists over voice loop and text messenger and picked and stowed the samples (see Fig. 1B). During a proficiency run on 18 November 2019, the astronaut visited one sampling site; during the main run on 25 November 2019, the astronaut visited all three. For interactions with these scientists and the remote robot, the astronaut (see Fig. 1C) was equipped with a laptop with a graphical user interface (GUI) as visualized in Fig. 1D, a custom-built joystick, and a space-qualified haptic device providing 6-DoF FF (*35*). These are described in more detail in Materials and Methods. During the proficiency run, the astronaut had direct voice contact with the Payload Developer (i.e., the robotics lead) at the European Astronaut Center (EAC), who was able to guide him through the interface. During the main run, the Payload Developer had no direct voice contact to the astronaut.

The average RTD was around 810 ms, and the average packet loss was 1.27% during the manipulation phases. The packet loss resulted from complete data loss or from jitter, i.e., delay variation, because only the latest packet was taken into account. Further data on the distribution of communication quality across the different sampling sites can be found in section S0.7.

Two frames of interaction were available to the operator. In base-frame interaction, the interaction frame of the input device I was mapped to the robot base frame R_B, whereas in tool-frame interaction (compare Fig. 2), the input device was mapped into the tool frame R_T. The robot was controlled in Cartesian impedance control (*36*), meaning that the torques on the robot result from a virtual (viscoelastic) impedance between the desired position ${}^{B}H_{R^{des}}$ and the current robot position ${}^{B}H_{R}$, rather than commanding positions to the joints. The interaction concept and the robot controller are further explained in sections S0.1 and S0.2.

The plots of the first picking at sampling site S2 are depicted in Fig. 2. Here, the motion of the input device ${}^{B}H_{I}$ in the negative x-axis direction commands a motion along the positive z axis of the tool frame R_T, which leads to a downward and slightly forward motion of the robot ${}^{B}H_{R}$ depending on the current tool orientation.

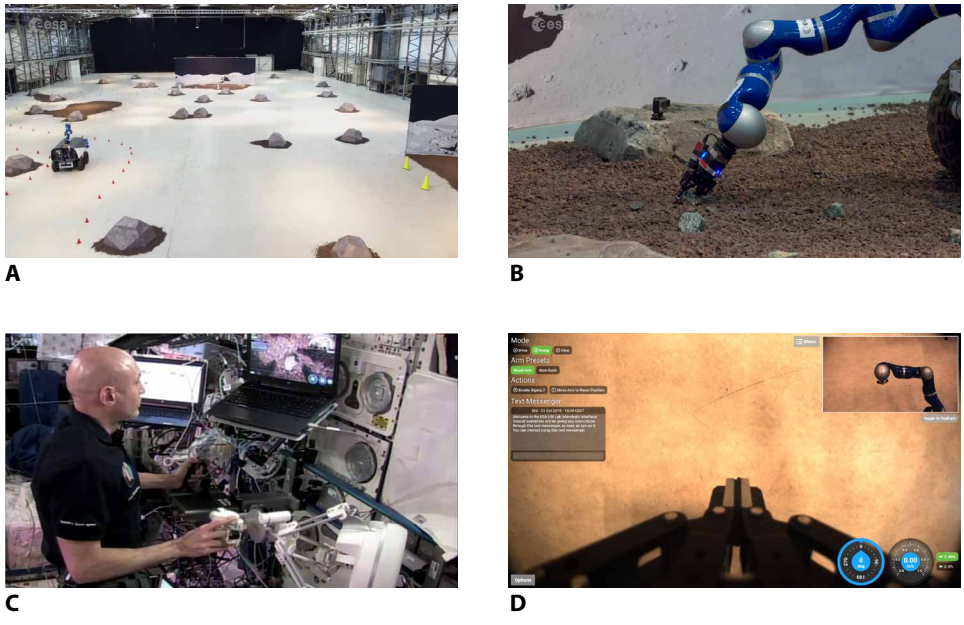

Fig. 1. Experimental scenario for the Analog-1 feasibility study. The rover with robotic manipulator is located on ground. The human operator aboard the ISS is equipped with a haptic input device and a GUI. (**A**) On-ground test environment. Three sampling sites and the predefined path marked with cones. (**B**) Robotic manipulator with gripper and rock sample. The robot is controlled to pick up a rock sample through direct teleoperation. (**C**) Astronaut on ISS. The astronaut is equipped with the space-qualified 6-DoF haptic interface sigma.7 and a custom-built joystick. (**D**) The GUI. In tool-frame interaction mode, the GUI presents the tool camera video stream in primary view with the overlaid head camera view.

Downloaded from https://www.science.org at The Hong Kong University of Science and Technology (Guangzhou) on May 25, 2026

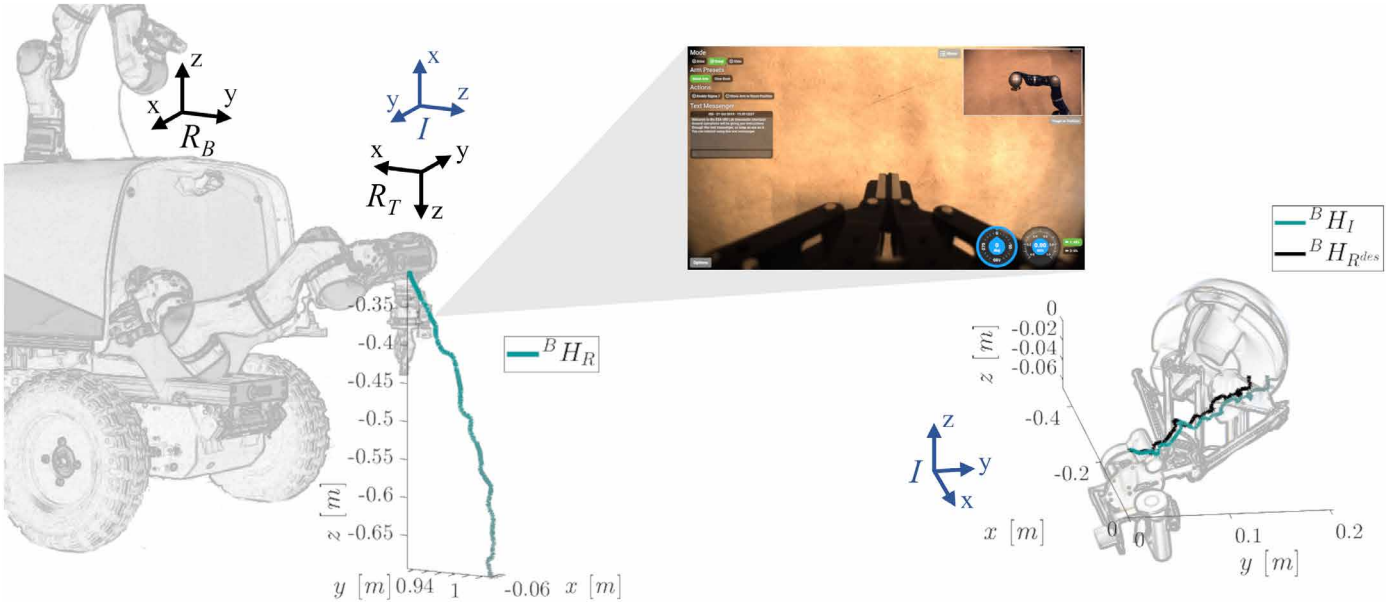

Fig. 2. Tool-frame interaction mode. Mapping the tool frame of the robotic manipulator R_T to the interaction frame of the FF device *I*.

Telemanipulation control

As previously discussed, FF telemanipulation at high delays requires measures such as additional damping to stabilize the closed loop coupling. The TDPA approach, with its adaptive damping, presents the state-of-the-art stabilization method in space teleoperation and has been tested successfully in abstract space experiments at different delay ranges. Nevertheless, TDPA [in its standard form (*37*)] leads to high position drift, which increases execution time, since the robot moves a shorter distance than commanded. Therefore, the standard TDPA is not optimal for tasks of high complexity involving large motions. Furthermore, hard impacts are not prevented intrinsically.

The TDPA method uses passivity observers to measure the energy transmission of the communication channel in the teleoperation system. If the output energy on one side [e.g., in local-to-remote (L2R) direction on the robot side E^{R}_{L2R}] is higher than the input energy on the respective other side (e.g., input device side E^{I}_{L2R}), passivity controllers (PCs) dissipate the excessive amount of energy through an adaptive damping. Thus, the energy E_{PC} after passivity control is lower than or equal to the respective input energy (e.g., E^{I}_{L2R}), and passivity, and hence unconditional stability, can be ensured.

In the standard TDPA, a power flow is measured even during free motion because the wrench (force and torque) generated by the coupling controller is considered in the energy analysis. This leads to excessive PC damping and position drift. A TDPA method for high delays (TDPA-HD) was developed and validated for the Analog-1 mission with the following requirements: [requirement (Req.) A] optimize position tracking accuracy, (Req. B) optimize FF quality, (Req. C) reduce execution time, and (Req. D) reduce severity of unintended impacts on the environment.

The conventional TDPA observes the energy flow from the velocity reference and the controller wrench. In contrast, the TDPA-HD considers the measured interaction wrench as FF and, crucially, also for energy observation and control. Thus, the transmitted wrench and the resulting energy flow during free motion is zero, and a contact phase can be clearly distinguished from free motion. As a result, the robot is stopped during the initial contact by the PC, reducing the severity of the impact. This and the related low position drift are the key properties of the TDPA-HD, directly fulfilling the aforementioned Req. A and Req. D. For implementation details on the 6-DoF control concept, the reader is referred to section S0.3.

The laboratory experiments presented in Fig. 3 compare a setup without stability control (no-TDPA) in Fig. 3A, the standard TDPA in Fig. 3B, and the developed approach TDPA-HD in Fig. 3C at 800-ms RTD. The controller parametrization of the laboratory and space setups can be found in section S0.4. The laboratory experiments were performed in base-frame interaction mode.

The plots in Fig. 3 present a free motion phase followed by a wall contact and another subsequent free motion phase. The plots are separated into the following phases: Over the first unshaded area, the devices are in free motion. During the first shaded area, the robot is in contact with the environment, but the operator has not perceived the contact yet. At the second shaded area, the operator perceives the contact with the environment with a 400-ms delay and presses against the contact, applying a power in this direction. After another 400 ms, over the third shaded area, the power applied by the operator (and thus the intention to interact with the environment) has arrived at the robot side. At the second unshaded area, the robot has released the wall contact.

Note that due to instability, the second unshaded area was not reached in the no-TDPA condition. Although the experiment was executed with 6-DoF devices, for the sake of brevity, the plots present the pose and force only in the *z* direction in which the free motion and wall contact were performed. The energy E^{R}_{R2L} enters and E^{I}_{R2L} exits the communication channel in R2L direction to the input device. Because of attenuation of the FF by the adaptive damping of the PC PCI (local PC), the energy E^{I}_{PC} exiting the passivity control in this direction is lower than E^{R}_{R2L} (compare Fig. 3, B and C), confirming the passivity of the communication channel. The same holds for the opposite direction, with input and output energies E^{I}_{L2R} and E^{R}_{L2R},

Downloaded from https://www.science.org at The Hong Kong University of Science and Technology (Guangzhou) on May 25, 2026

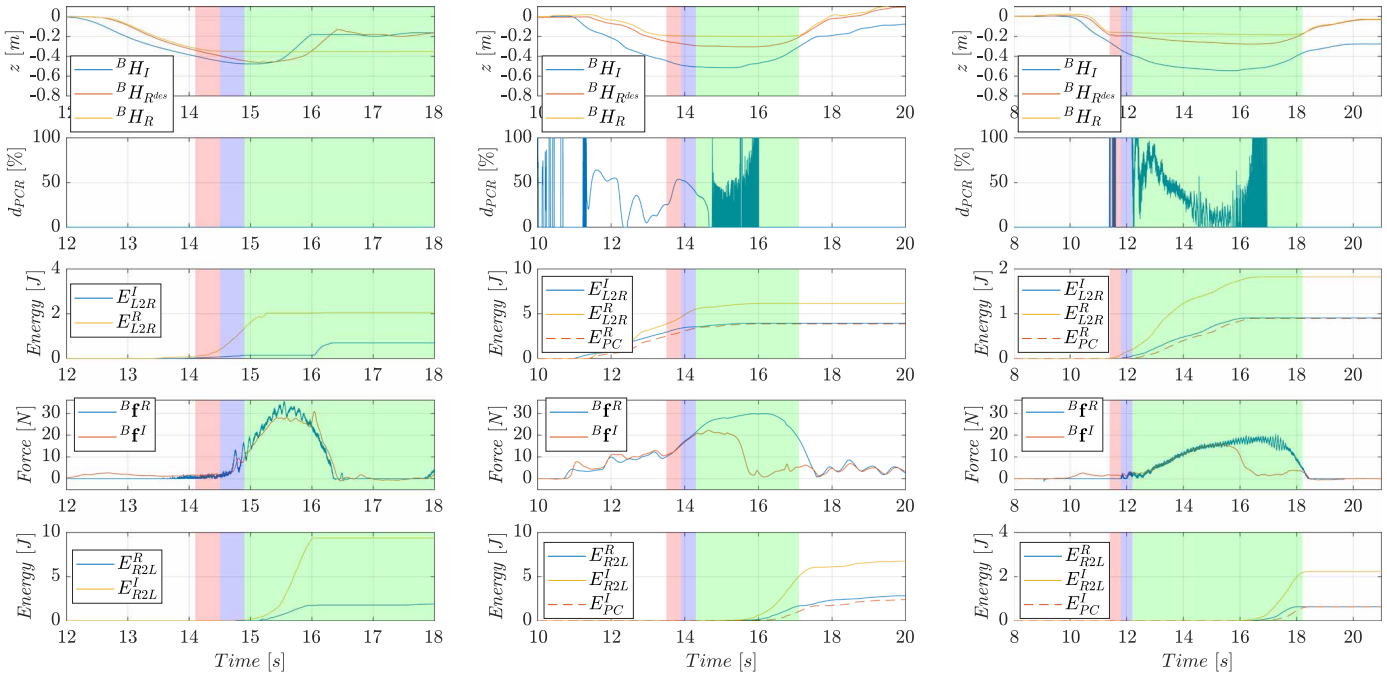

Fig. 3. Results of the laboratory experiments with TDPA and TDPA-HD. Comparison of control with no-TDPA (**A**), TDPA (**B**), and TDPA-HD (**C**) at 800-ms round-trip delay, regarding position tracking accuracy, FF quality, and severity of impacts.

and the energy output E^{R}_{PC} after the PC PCR (remote PC) has attenuated the twist reference sent to the robot side. The energies result from the respective wrench and twist as described in section S0.3. The variable d_{PCR} is the percentage attenuation of P^{R}_{L2R} by the PC.

Position tracking

One of the major drawbacks of the standard TDPA is the position drift during free motion. The velocity command is attenuated by the robot-side PC PCR, and this attenuation leads to a growing position offset (or drift) between input device ${}^{B}H_{I}$ and robot reference pose ${}^{B}H_{R}{}^{des}$.

The plot of the percentage of dissipated power d_{PCR} highlights the fact that the PCR dissipates energy during free motion only in the case of TDPA. This leads to a large position drift at t = 13 s (see Fig. 3B). In contrast, in the TDPA-HD and no-TDPA cases, the difference between desired robot pose ${}^{B}H_{R}{}^{des}$ and input device pose ${}^{B}H_{I}$ before the wall contact results purely from the delay [see Fig. 3A (t = 14.2 s) and Fig. 3C (t = 11.6 s)]. The position drift in TDPA leads to low position tracking accuracy (Req. A) and increased execution time (Req. C), because the input device has to be moved longer to achieve the desired pose change of the robot. In the free motion phase (first unshaded area), the movement of the robot is 59% shorter than commanded due to position drift in TDPA, whereas the drift is below 1% for TDPA-HD. Because the workspace of the ISS input device is smaller than that of the robot, the input device must be decoupled and moved to a reset position (indexing) when input workspace limits are reached. Position drift increases the frequency at which indexing is needed.

Safe interactions

In contrast to TDPA, in TDPA-HD, the PCR varies the velocity command only during interaction with the environment, i.e., when the measured external wrench is nonzero. In free motion, the measured wrench is zero; thus, no power is registered and no energy needs to be dissipated.

Because the robot-side PC PCR only dissipates energy when energy is flowing from input device to robot, for TDPA-HD, drift especially appears in the initial impact phase of a contact (first and second shaded area). Therefore, in Fig. 3C, the drift appears until the human operator feels the force from the interaction (delayed because of the latency of the communication channel) and intentionally commands a velocity against this force. Thus, TDPA-HD prevents hard unexpected impacts (Req. D) on the environment, because due to the reduced velocity command, the initial interaction force is also limited. This is especially important at high delays, when the operator is not instantaneously informed visually or haptically about an impending collision.

In contrast, in the case of no-TDPA, the robot collided with the environment without any safety precautions, meaning that the low-level safety measures stopped the robot at t = 15 s to prevent hardware damage. With the standard TDPA, the collision is only damped by the consistently present position drift, but the controller cannot distinguish between free motion and contact, because the energy flow analysis uses computed forces, not measured forces.

Force-feedback

In the case of no-TDPA (see Fig. 3A), the position accuracy is high and the FF is not altered, but the input device is strongly pushed back from contact because the robot applies more force than expected by the operator. This active behavior would result in instability, for instance, if the robot was located between two contacts (not depicted). During the releasing phase of the wall contact in particular (maximal penetration at around t = 15 s in Fig. 3, B and C), the PCI reduces

Downloaded from https://www.science.org at The Hong Kong University of Science and Technology (Guangzhou) on May 25, 2026

the feedback force ${}^{B}\mathbf{f}^{R}$ more in TDPA than in TDPA-HD. A passive filter (*38*) has been applied to filter the high-frequency force output of the PC. In the case of TDPA, the force during contact was reduced by 47%, and for TDPA-HD by 36%. It should, however, be noted that, in general, the PCI is expected to yield equivalent force reduction for both TDPA and TDPA-HD. Because PC dissipation depends on velocity, comparable velocities were applied for TDPA and TDPA-HD.

Development outcome

Stable telemanipulation can be achieved with TDPA and TDPA-HD. Drift during free motion can only be avoided with TDPA-HD under stable conditions. The drift of the standard TDPA increases with time delay and with noncontinuity of the commanded velocity, which clearly increases the execution time in realistic scenarios requiring large motions. The drift appears for TDPA-HD only during the initial contact phase, which results in safe interactions in contrast to the TDPA and no-TDPA setup.

In addition to this laboratory evaluation, an on-ground sample-picking user study confirmed that, through TDPA-HD, impact forces and position drift as well as execution time are significantly reduced when compared to TDPA. The design and the results of this user study are presented in detail in section S0.5.

Teleoperated sample picking with FF

Although both base-frame and tool-frame interactions were available to the operator as previously described, during sample collection in the space experiments only tool-frame interaction was chosen. Most samples were well visible due to their larger size compared to the gravel, except the first pick at the third sampling site (S3-1), where the astronaut was instructed to grasp a smaller rock from a field of similar rocks. The operator needed 10 grasps for six samples during the main run. Different performance metrics for the two sample pickings (1 and 2) at each sampling site (S1, S2, and S3) of the space experiment and the proficiency run (*P*-1, *P*-2) and a picture sequence of an exemplary sampling procedure *S*1-1 can be found in section S0.8. During the first sample picking of the proficiency run *P*-1 and the real experiment, the object was not hit on the first try. The first grasp initiated by the astronaut during S1-1 was unsuccessful, because the gripper was positioned too high above the sample due to poor depth information from mono vision. One sample was dropped intentionally by the operator, one dropped during operator motion, and one dropped during the automatic stowing.

A representative picking procedure

The following analysis of the space-to-ground telemanipulation performance is based on the data of the first sample picking in the second sampling site S2-1. Figure 2 presents the translational information, whereas the orientation can be found in section S0.9 for the sake of completeness. Figure 2 presents the respective three-dimensional (3D) motion plots for times between t = 2000 s and t = 2052 s.

Figure 4A depicts the robot pose ${}^{B}H_{\mathrm{R}}$ and the desired/reference pose ${}^{B}H_{\mathrm{R}^{\mathrm{des}}}$. Because tool-frame interaction was used by the astronaut, velocities of the input device were commanded to the device in the constantly changing tool frame; thus, positions and orientations cannot be compared side by side. To discuss the effect of passivity control in more detail, the energies and the path of input device and robot during the contact phase are presented additionally in Fig. 5 for times between t = 2052 s and t = 2064 s. Because the passivity control took place in the tool frame of the robot R_{T}, the energies of Fig. 4 (C and D) refer to the input device frame *I*. The forces of Fig. 4B are presented in the robot base frame R_{B}.

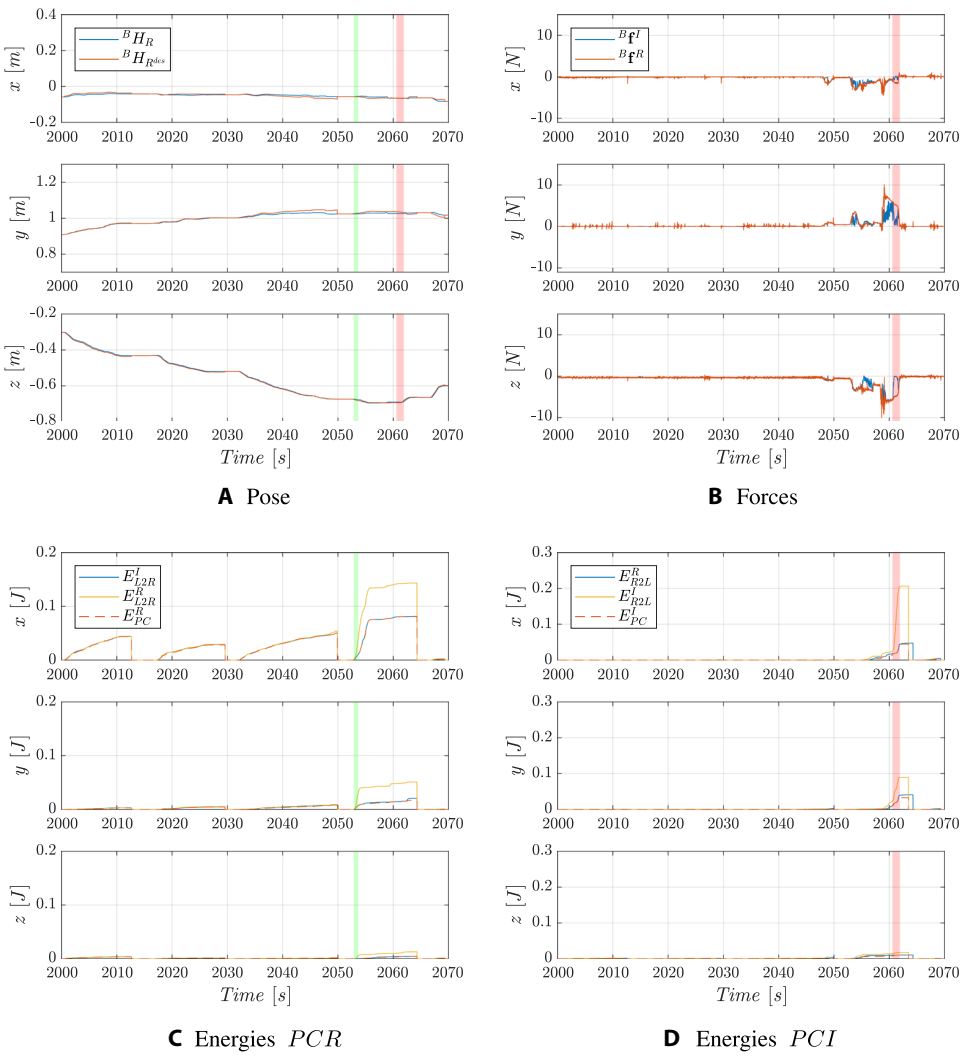

Fig. 4. Results of the Analog-1 feasibility study. Analysis of position tracking (**A**) and FF quality (**B**) in translations for the first rock sample picking S2-1 in sampling site 2. The energies (**C** and **D**) present the behavior of the remote PC (PCR) and local PC (PCI).

Downloaded from https://www.science.org at The Hong Kong University of Science and Technology (Guangzhou) on May 25, 2026

The robot arm was moved in a stepwise manner (due to indexing) downward (negative z direction) and slightly forward (positive y direction). Upon contact of the robotic manipulator with its environment, this resulted in reaction forces in these directions (see Fig. 4B). The motion was commanded in the negative x and positive y directions in the input device frame I (compare Fig. 2).

The robot's position ${}^{B}H_{\mathrm{R}}$ tracks the commanded position ${}^{B}H_{\mathrm{R}}{}^{\mathrm{des}}$ using a virtual Cartesian impedance, but joint-level impedances deflect the joints away from limits or singularity (more details in section S0.2). Where tracking is poor, this may be due to contact with the ground or due to the robot approaching joint limits or a singularity position.

Indexing was activated five times during the sampling approach S2-1. The final indexing at t = 2050 s was activated after the astronaut has perceived the initial contact to reconfigure the input device and to optimize the workspace for the approach to the sample. The indexing was initiated through a release of the astronaut's button interface leading to an energy reset and a reset of ${}^{B}H_{\mathrm{R}}{}^{\mathrm{des}}$ to ${}^{B}H_{\mathrm{R}}$. Because of this reset of the reference pose, the controller spring is unloaded such that the wrench acting on the robot was set to zero during indexing (t = 2050 s to 2052 s). The energy plots show that E_{PC} was mostly very close to the input energies $E^{\mathrm{R}}_{\mathrm{R2L}}$ and $E^{\mathrm{I}}_{\mathrm{L2R}}$. As expected, PCR mainly dissipated energy during the initial contact phase at t = 2050.8 s to 2053.6 s (light shaded area) and PCI mainly dissipated during the release of the contact (dark shaded area) with the environment at t = 2060 s to 2062 s.

The path plots in Figs. 4A and 5A depict the input device path$_{\mathrm{I}}$ and the robot path$_{\mathrm{R}}$, which is the time integral of the absolute translational velocity vector length of the respective device. Note that the path plots start at zero for each plot for ease of analysis. The path and energy plots confirm that the main position drift occurred during the initial impact (light shaded area). Through this drift, the severity of the impact was reduced (Req. D). Apart from the impact situation, the dissipation by PCR and thus the drift was very low; i.e., Req. A and Req. C for high position tracking accuracy and reduction of execution time were achieved in the space experiment.

The plots of Fig. 4B show that the feedback wrench during free motion was negligibly low, resulting in a comfortable unhindered motion command. As expected, PCI reduced the FF mainly during release of the contact with the environment (dark shaded area in Fig. 5B) when energy flows from the robot to the input device side. As long as energy flows to the robot, no dissipation or adaptation of the feedback wrench is required on the input device side. The plot of the force vector lengths shows that the forces displayed on the input device $\|{}^{B}\mathbf{f}^{\mathrm{I}}\|$ were very similar to the measured wrench $\|{}^{B}\mathbf{f}^{\mathrm{R}}\|$ until the contact is released at t = 2061 s. Figure 6 depicts the robot's trajectory with solid vectors of measured forces and dashed vectors of the forces displayed on the haptic input device. It can be analyzed that despite the variation through passivity control, the feedback forces indicated the contact well during pressing and also releasing (Req. B), although the direction of the force was slightly altered because of DoF-specific passivity control. After the teleoperated picking of the rock sample, the astronaut commanded autonomous stowing of the sample via the GUI.

DISCUSSION

In addition to the verification of feasibility of space-to-ground telemanipulation under real spaceflight conditions, several observations on the user and system performance can be drawn from the objective and subjective data.

The following observations can be drawn from the objective data. Despite high delay and packet loss, the astronaut was able to collect all samples except for the last sample, which was lost during the automated stowing. Our control approach prevents hard impacts (Req. D) and enables high FF quality (Req. B). A clear distinction can be made between contact and free motion: Because we use measured FF for passivity observation and control, no forces are transmitted during free motion that might disturb the operator. Furthermore, the position drift in free motion is clearly reduced through TDPA-HD such that the execution time (Req. C) and the associated workload of the operator are reduced. In addition, a high position tracking quality (Req. A) is achieved because the rigidity of the coupling controller can be set independently of the TDPA-HD and delay.

Regarding the effects of the high delay, the force plots show low levels of dissipation and adaptive damping, i.e., minimal interference in the teleoperation from the TDPA-HD. In contrast, stabilizing a no-TDPA setup with nonadaptive control strategies would require high continual damping in the Analog-1 delay range.

During the space experiment, the indexing method was used to extend the workspace of the input device and to bring the input device into a comfortable initial position to approach the grasping pose. Considering that the horizontal workspace of the input device is 0.17 m, on average, 72% of the indexing steps were required only due to the translational workspace limitation. Further indexing steps were required for adaptation of the robotic gripper pose. The small proportion of indexing performed for other reasons, such as tentativeness or hesitancy, suggest that the operator had sufficiently low mental workload to

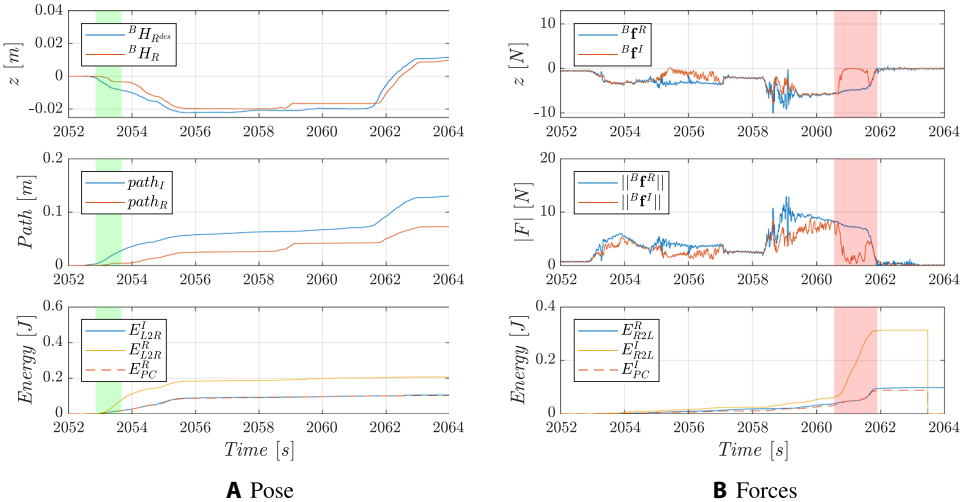

A Pose **B** Forces

Fig. 5. Performance during contacts in the Analog-1 experiment. Detailed analysis of position drift (**A**) and impact behavior (**B**) for the first rock sample picking S2-1 in sampling site 2.

Downloaded from https://www.science.org at The Hong Kong University of Science and Technology (Guangzhou) on May 25, 2026

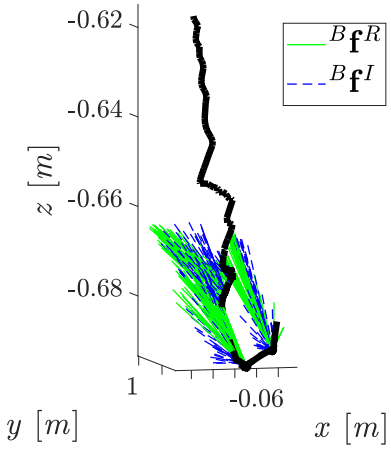

Fig. 6. 3D plot of manipulator motion and interaction forces. The figure depicts the height and direction of the force $^B\mathbf{f}^I$ displayed at the FF device and the force $^B\mathbf{f}^R$ measured at the robotic manipulator during the S2-1 contact.

work in a focused manner. This is further supported by the crew questionnaire results discussed later.

The performance data presented in section S0.8 indicates that the astronaut learned the sample picking very fast, because the number of indexing steps, the time (both in relation to the path length), and the maximum forces rapidly decreased in the proficiency run after the first sample *P*-1. A similar but less pronounced training effect can be observed for the first sample picking of the main space experiment S1-1. Here, the mean force, the number of wrong grasps, and the high position drift are higher than in the later sample pickings. During S3-1, more interaction with the environment was required, whereas the increased forces during *P*-1 and S1-1 might hint that the operator initially interacted with the environment more carelessly. This analysis is substantiated by the high drift of *P*-1 and S1-1, which mainly results from the impacts of the robotic manipulator on the environment.

The average velocity was similar over all sample pickings. Overall, the execution speed was higher than previously expected, considering the high delay and weak visual feedback. From this objective data, it can be deduced that the astronaut felt comfortable with the task and the user interface for haptic interaction.

These objective results correspond with subjective data gathered through a questionnaire (see section S0.10). Subjective workload ratings were comparably low (6 on a scale ranging from 1 to 20), and a good level of situational awareness was reported despite the complexity of the task, the substantial time delay, various sources of information, and the restricted video quality (providing no depth information). Regarding the sense of presence or immersion, the astronaut indicated that interacting with the remote environment does not feel artificial and that the control mechanism is intuitive to use. However, the astronaut noted that additional information from the remote site (e.g., distance from the robot end effector to ground and a laser pointer on the robotic arm) should be available to improve spatial perception.

Further feedback related to the operator's focus and attention indicated that the interface should be based on as few different devices as possible and that a touchscreen is preferable to a combination of laptop button and mouse. This provides support to recent developments in space user interfaces, e.g., (*39*). The astronaut also remarked that using the 6-DoF device for telenavigation would eliminate the need to switch back and forth from the 3-DoF joystick, thus reducing the operator's workload.

As a realistic case study, the Analog-1 space experiment delivered valuable insights into the space-to-ground teleoperation of a mobile robot on a planet's surface from orbit. Specific design rules of the user interface that are studied in more detail in (*35*) were deduced from the training sessions and the space experiments. As few devices as possible should be used to simplify the interface and to avoid the distractive switching between devices, all while providing access to all functionalities.

During the laboratory validation with simulated space-like communication links, the deficiencies of the state-of-the-art telemanipulation control approaches were revealed, which led to the development of a control approach assuring sufficient position tracking accuracy and safe interactions despite high delays, packet loss, and limited bandwidth. The objective and subjective results underline the high performance of the developed haptic control loop, which allowed for a natural and intuitive interaction. Further improvements of the control method are discussed in the subsequent section. The robot controller was parametrized to be relatively compliant, but the developed controller also guarantees stability and safe interactions in case of stiffer parametrization for other tasks requiring even higher precision.

The experiment as a feasibility study confirms the suitability of the system architecture including robotic hardware, communication, and the interaction design for a space-to-ground exploration scenario. Although no indication was found that spaceflight conditions (microgravity, mental and physical workload, etc.) had any effect on teleoperation performance, the interpretation of the related results is limited because of the experiment's nature as a feasibility study. Potential effects of the adaptation to microgravity in the early phase of an astronaut's space mission, however, were circumvented because the astronaut had been in space already for 121 days during the proficiency run and 128 days during the main run.

The subjective and objective results of this case study give insight into the high degree of transparency of the interaction concept. In the simulated Earth surface–to–Lunar surface experiment (*40*), the developed approach was already successfully tested for sliding, insertion, rock sampling, and maintenance tasks at 3-s RTD. Current ambitions of robots on the Moon teleoperated from the Lunar Orbital Platform-Gateway (LOPG) involve delays in the range of seconds. There, the developed approach will be required for safe interactions independent of the needs for kinesthetic FF.

Besides the haptic data, visual feedback is important for optimal performance in interaction. Whereas the Analog-1 mission displayed two camera views on a computer screen, other space projects make use of head-mounted displays to enhance the astronaut's immersion during virtual-reality on-board training (*41*). Although time delay is not considered here, results from these experiments can help to understand how an immersive experience can be recreated in microgravity.

The performance of the developed control concepts, which requires a dead zone of the measured feedback force, will be further enhanced in future work. With increasing weight of the object, a drift may result, though not observed during this mission. The observation and compensation of the load's weight in the user feedback can reduce a potential drift, and the observed weight can be dynamically simulated locally on the input device.

Downloaded from https://www.science.org at The Hong Kong University of Science and Technology (Guangzhou) on May 25, 2026

Fig. 7. Close-up view on the setup aboard the ISS. Space-qualified haptic interfaces on the ISS including the FF device sigma.7 and the custom-built joystick.

Fig. 8. On-ground setup. The all-terrain, four-wheel drive rover with two robotic manipulators for sample picking and head camera motion, respectively.

A more obvious limitation of the experiment is the Lunar analog environment of the rover, which was not realistic in terms of terrain. As part of the ARCHES campaign (*42*) in summer 2022, the same ISS crew will repeat the experiment on ground (operator in 1*g* gravity without hard time constraint), as part of an extensive campaign on the volcano Etna. Thus, the geological conditions and outdoor environmental task complexity of a Moon mission will be replicated. Because the terrain will be uneven and sloping, the variability of the gravity vector will need to be considered.

A 6-DoF extension of the passive filter (*38*) was developed and applied in the laboratory experiments. Because this filter adds another mass coupling on the input device and the robot, it needs to be extensively tested; in light of the limited testing opportunities due to an inflexible ISS-determined time scale, a low-pass filter was applied instead. Also, the velocity used for power calculation was filtered with a standard low-pass filter to avoid unexpected effects of the unknown nature of the space-ground link.

The benefits of the safety aspects of the TDPA-HD approach are not limited to space exploration. For example, they can also be transferred into tele–health care assistance robotics. Independent of the delay, the limitation of power transmission to the robot's environment in case of unexpected contacts can help to ensure safety in human-robot shared environments. This can also form the basis for new safety standards in teleoperated and autonomous robotics.

MATERIALS AND METHODS

System architecture and communication

The ISS is located in low-Earth orbit (LEO), only 320 to 430 km above Earth. This means that, for any given location on Earth's surface, it is below the horizon for most of its 90-min orbit and therefore unreachable. For that reason, the data were transmitted over KU-band via the Tracking and Data Relay Satellite System. These are three clusters of satellites in geostationary orbit (35,700 km above Earth) from which both the ISS and NASA's White Sands Satellite Complex in the United States are always visible. From the White Sands, the communication passes via a transatlantic cable to Germany and the ground site in The Netherlands.

The link had an RTD of up to 850 ms, was severely bandwidth-limited (4 Mbps in both directions), and required a communication protocol/middleware that is able to handle a DIL (Disconnected, Intermittent or Lossy) communication link (RTI Connext DDS based on UDP/IP).

The down-link was mainly dedicated for real-time robot control commands (at 167 Hz), whereas the up-link bandwidth consisted of real-time sensor information of the robot (also at 167 Hz) and two

Downloaded from https://www.science.org at The Hong Kong University of Science and Technology (Guangzhou) on May 25, 2026

video streams. To achieve sufficient video quality in terms of resolution and frames per second, two GStreamer pipelines were implemented encoding the mono videos into the H.264 format at low frequency (12 to 15 Hz).

Robotic setup and methodology for replication

The orbiter setup

The user interface on the orbiter ISS depicted in Fig. 1C consisted of a laptop for the GUI; the adapted commercial FF device sigma.7 from Force Dimension; and a custom-built joystick for telenavigation of the mobile robotic platform, movement of the rover head camera, stabilizing the operator, and enabling sigma.7 (see Fig. 7).

Because of its low dynamic mass and the rigid parallel base structure, the sigma.7 device is able to provide high-fidelity FF on all six Cartesian DoF and an additional actuated gripper. The modifications to achieve compliance with ISS payload safety requirements included the replacement of casing materials, noncompliant internal electrical components, and adaptations of the power connector. The internal springs, required for gravity compensation, were also removed.

To operate sigma.7, the operator had to grasp the handle on the custom-built joystick and press the integrated "enable" button to activate FF and command motion. The handle was also for stabilization in microgravity against the FF: The astronaut could exert a reaction force on it. In addition, the astronaut could stabilize his posture through feet restraints.

The GUI (compare Fig. 1D) provided information on the active control mode (driving, grasping, viewing), rover speed, rover heading, battery status, and a grid overlay. Furthermore, a text messenger to communicate with the science team on ground was available, and two camera feeds presented the view from the rover head and tool cameras. A settings drawer allowed the adaptation of the rover top speed, the activation or deactivation of widgets, and a connectivity check of the devices. A digital user manual and the questionnaire for gathering of subjective data on user experience were integrated into the GUI.

The ground setup

The Interact Rover platform depicted in Fig. 8 was built upon a commercial locomotion system (AMBOT GRP-4400) with an all-terrain chassis with four-wheel drive, allowing Ackermann steering and spot turns. The rover was equipped with two KUKA 7-DoF LWR4+ manipulators. The robotic arm mounted on top of the rover served the positioning of the head camera, which could be adjusted via the custom joystick. The second arm on the rover front was used for telemanipulation and had an auxiliary camera mounted near the tool. A six-axis ATI force-torque sensor was mounted on the seventh joint and a Robotiq 2-finger gripper after it.

The laboratory experiments, shown in Fig. 3, were also performed with two KUKA 7-DoF LWR4+ manipulators. The communication channel was simulated with a constant delay and without packet loss.

The real-time software was running on a real-time Linux system (OpenSuse Leap 42.3 Preempt RT for the laboratory experiments and the robot arms in the space experiment, and a custom-built Debian-based system with Xenomai for the ISS control station) at a 1-kHz sampling rate.

SUPPLEMENTARY MATERIALS

www.science.org/doi/10.1126/scirobotics.abl6307
Interaction frames for robot control
Cartesian impedance control
Figs. S1 to S7
Tables S1 to S9
Controller parametrization
Statistical evaluation of TDPA-HD
Implementation challenges and solutions
Communication data
Performance data and metrics
Experimental data
Questionnaire responses
References (*43*–*56*)

REFERENCES AND NOTES

1. J. A. Crisp, M. Adler, J. R. Matijevic, S. W. Squyres, R. E. Arvidson, D. M. Kass, Mars exploration rover mission. *J. Geophys. Res.* **108**, 8061 (2003).
2. K.-H. Glassmeier, H. Boehnhardt, D. Koschny, E. Kührt, I. Richter, The Rosetta mission: Flying towards the origin of the solar system. *Space Sci. Rev.* **128**, 1–21 (2007).
3. Y. Gao, S. Chien, Review on space robotics: Toward top-level science through space exploration. *Sci. Robot.* **2**, eaan5074 (2017).
4. D. S. Lauretta, S. S. Balram-Knutson, E. Beshore, W. V. Boynton, C. D. d'Aubigny, D. N. D. Giustina, H. L. Enos, D. R. Golish, C. W. Hergenrother, E. S. Howell, C. A. Bennett, E. T. Morton, M. C. Nolan, B. Rizk, H. L. Roper, A. E. Bartels, B. J. Bos, J. P. Dworkin, D. E. Highsmith, D. A. Lorenz, L. F. Lim, R. Mink, M. C. Moreau, J. A. Nuth, D. C. Reuter, A. A. Simon, E. B. Bierhaus, B. H. Bryan, R. Ballouz, O. S. Barnouin, R. P. Binzel, W. F. Bottke, V. E. Hamilton, K. J. Walsh, S. R. Chesley, P. R. Christensen, B. E. Clark, H. C. Connolly, M. K. Crombie, M. G. Daly, J. P. Emery, T. J. M. Coy, J. W. M. Mahon, D. J. Scheeres, S. Messenger, K. Nakamura-Messenger, K. Righter, S. A. Sandford, OSIRIS-REx: Sample return from asteroid (101955) Bennu. *Space Sci. Rev.* **212**, 925–984 (2017).
5. H.-J. Sedlmayr, S. Barthelmes, R. Bayer, W. Bertleff, M. Bihler, F. Buse, M. Chalon, D. Franke, MMX-development of a rover locomotion system for Phobos, in *Proceedings of the 2020 IEEE Aerospace Conference* (IEEE, 2020), pp. 1–10.
6. N. Y. Lii, C. Riecke, D. Leidner, S. Schätzle, P. Schmaus, B. Weber, T. Krueger, M. Stelzer, A. Wedler, G. Grunwald, The robot as an avatar or co-worker? An investigation of the different teleoperation modalities through the Kontur-2 and METERON SUPVIS Justin space telerobotic missions, in *Proceedings of the International Astronautical Congress* (IAF, 2018).
7. R. Ambrose, I. A. D. Nesnas, F. Chandler, B. D. Allen, T. Fong, L. Matthies, R. Mueller, *NASA Technology Roadmaps: TA 4: Robotics and Autonomous Systems* (NASA, 2015).
8. V. Nitsch, B. Färber, A meta-analysis of the effects of haptic interfaces on task performance with teleoperation systems. *IEEE Trans. Haptics* **6**, 387–398 (2012).
9. B. Weber, C. Eichberger, The benefits of haptic feedback in telesurgery and other teleoperation systems: A meta-analysis, in *International Conference on Universal Access in Human-Computer Interaction* (Springer, 2015), pp. 394–405.
10. J. C. D. A. Fletcher, F. J. Greeb, S. B. Brodie, C. R. Flatau, Variable ratio mixed-mode bilateral master-slave control system for shuttle remote manipulator system. U.S. Patent 3,893,573 (1975).
11. A. Lippay, Multi-axis hand controller for the shuttle remote manipulator system, in *MIT Proceedings of the 13th Annual Conference on Manual Control* (MIT, 1977).
12. G. Hirzinger, B. Brunner, J. Dietrich, J. Heindl, ROTEX—The first remotely controlled robot in space, in *Proceedings of the 1994 IEEE International Conference on Robotics and Automation* (IEEE, 1994), pp. 2604–2611.
13. F. Peñìn, K. Matsumoto, S. Wakabayashi, ETS-7 space robot teleoperation through virtual force reflection, in *Artificial Intelligence, Robotics and Automation in Space* (ESA Special Publication, 1999).
14. K. Landzettel, B. Brunner, K. Deutrich, G. Hirzinger, G. Schreiber, B. M. Steinmetz, DLR/NASDA's joint robotics experiments on ETS-VII, in *ETS VII Symposium* (NASDA, 2000), vol. 14, p. 2000.
15. C. Sallaberger; Space Plan Task Force, Canadian Space Agency, Canadian space robotic activities. *Acta Astronaut.* **41**, 239–246 (1997).
16. T. Imaida, Y. Yokokohji, T. Doi, M. Oda, T. Yoshikawa, Ground-space bilateral teleoperation of ETS-VII robot arm by direct bilateral coupling under 7-s time delay condition. *IEEE Trans. Robot. Autom.* **20**, 499–511 (2004).
17. G. Hirzinger, K. Landzettel, D. Reintsema, C. Preusche, A. Albu-Schäffer, B Rebele, M. Turk, ROKVISS—Robotics component verification on ISS, in *Proceedings of the International Symposium on Artificial Intelligence, Robotics and Automation in Space (iSAIRAS)* (ESA, 2005).
18. A. Schiele, Towards the interact space experiment: Controlling an outdoor robot on earth's surface from space, in *Proceedings of the 13th Symposium on Advanced Space Technologies for Robotics and Automation (ASTRA)* (ESA, 2015).
19. C. Riecke, J. Artigas, R. Balachandran, R. Bayer, A. Beyer, B. Brunner, J. Buchner, T. Gumpert, R. Gruber, F. Hacker, K. Landzettel, G. Plank, S. Schätzle, H.-J. Sedlmayr, N. Seitz, B.-M. Steinmetz, M. Stelzer, J. Vogel, W. Weber, B. Willberg, A. O. Albu-Schäffer, Kontur-2 mission: The DLR force feedback joystick for space telemanipulation from the ISS, in *The International Symposium on Artificial Intelligence, Robotics and Automation in Space (i-SAIRAS)* (China National Space Administration, 2016).
20. B. Weber, R. Balachandran, C. Riecke, F. Stulp, M. Stelzer, Teleoperating robots from the International Space Station: Microgravity effects on performance with force feedback, in *Proceedings of International Conference on Intelligent Robots and Systems (IROS)* (IEEE, 2019).

Downloaded from https://www.science.org at The Hong Kong University of Science and Technology (Guangzhou) on May 25, 2026

21. M. Panzirsch, R. Balachandran, J. Artigas, C. Riecke, M. Ferre, A. Albu-Schäffer, Haptic intention augmentation for cooperative teleoperation, in *Proceedings of 2016 IEEE International Conference on Robotics and Automation* (IEEE, 2017), pp. 5335–5341.
22. J. Artigas, R. Balachandran, M. De Stefano, M. Panzirsch, R. Lampariello, A. Albu-Schäffer, J. Harder, J. Letschnik, Teleoperation for on-orbit servicing missions through the ASTRA geostationary satellite, in *Proceedings of 2016 IEEE Aerospace Conference* (IEEE, 2016), pp. 1–12.
23. L. F. Peñìn, K. Matsumoto, S. Wakabayashi, Force reflection for time-delayed teleoperation of space robots, in *Proceedings 2000 ICRA. Millennium Conference. IEEE International Conference on Robotics and Automation* (IEEE, 2000), vol. 4, pp. 3120–3125.
24. C. Borst, T. Wimböck, F. Schmidt, M. Fuchs, B. Brunner, F. Zacharias, P. R. Giordano, R. Konietschke, W. Sepp, S. Fuchs, C. Rink, A. Albu-Schäffer, G. Hirzinger, Rollin' Justin—Mobile platform with variable base, in *2009 IEEE International Conference on Robotics and Automation* (IEEE, 2009), pp. 1597–1598.
25. P. Schmaus, D. Leidner, T. Krueger, A. Schiele, B. Pleintinger, R. Bayer, N. Y. Lii, Preliminary insights from the METERON SUPVIS Justin space-robotics experiment. *IEEE Robot. Autom. Lett.* **3**, 3836–3843 (2018).
26. J.-H. Ryu, D.-S. Kwon, B. Hannaford, Stable teleoperation with time-domain passivity control. *Trans. Robot. Autom.* **20**, 365–373 (2004).
27. G. D. Niemeyer, "Using wave variables in time delayed force reflecting teleoperation," thesis, Massachusetts Institute of Technology, Cambridge, MA (1996).
28. R. Balachandran, J. Artigas, U. Mehmood, J.-H. Ryu, Performance comparison of wave variable transformation and time domain passivity approaches for time-delayed teleoperation: Preliminary results, in *Proceedings of 2016 IEEE/RSJ International Conference on Intelligent Robots and Systems* (IEEE, 2016), pp. 410–417.
29. A. Schiele, M. Aiple, T. Krueger, F. van der Hulst, S. Kimmer, J. Smisek, E. den Exter, Haptics-1: Preliminary results from the first stiffness JND identification experiment in space, in *International Conference on Human Haptic Sensing and Touch Enabled Computer Applications* (Springer, 2016), pp. 13–22.
30. J. Rebelo, A. Schiele, Time domain passivity controller for 4-channel time-delay bilateral teleoperation. *IEEE Trans. Haptics* **8**, 79–89 (2015).
31. J. Artigas, R. Balachandran, C. Riecke, M. Stelzer, B. Weber, J.-H. Ryu, A. Albu-Schäffer, Kontur-2: Force-feedback teleoperation from the International Space Station, in *Proceedings of 2016 IEEE International Conference on Robotics and Automation (ICRA)* (IEEE, 2016), pp. 1166–1173.
32. N. Kanas, D. Manzey, *Space Psychology and Psychiatry* (Springer, 2008).
33. B. Weber, C. Riecke, F. Stulp, Sensorimotor impairment and haptic support in microgravity. *Exp. Brain Res.* **239**, 967–981 (2021).
34. K. Wormnes, W. Carey, T. Krueger, L. Cencetti, E. den Exter, S. Ennis, E. Ferreira, A. Fortunato, L. Gerdes, L. Hann, C. Lombardi, E. Luzzi, S. Martin, M. Massironi, S. Payler, A. Pereira, A. P. Rossi, R. Pozzobon, F. Sauro, P. Schoonejans, F. van der Hulst, J. Grenouilleau, ANALOG-1 ISS—The first part of an analogue mission to guide ESA's robotic moon exploration efforts, in *Global Space Exploration Conference (GLEX 2021)* (International Astronautical Federation, 2021).
35. T. Krueger, E. Ferreira, A. Gherghescu, L. Hann, E. den Exter, F. van der Hulst, L. Gerdes, L. Cencetti, A. Pereira, H. Singh, M. Panzirsch, T. Hulin, R. Balachandran, B. Weber, N. Y. Lii, Designing and testing a robotic avatar for space-to-ground teleoperation: The developers' insights, in *Proceedings of the International Astronautical Congress* (IAC IAF, 2020).
36. A. Albu-Schäffer, C. Ott, G. A. Hirzinger, Unified passivity-based control framework for position, torque and impedance control of flexible joint robots. *Int. J. Robot. Res.* **26**, 23–39 (2007).
37. J. Artigas, C. Preusche, G. Hirzinger, Time domain passivity for delayed haptic telepresence with energy reference, in *2007 IEEE/RSJ International Conference on Intelligent Robots and Systems* (IEEE, 2007), pp. 1612–1617.
38. J.-H. Ryu, J. Artigas, C. Preusche, A passive bilateral control scheme for a teleoperator with time-varying communication delay. *Mechatronics* **20**, 812–823 (2010).
39. C. Gohd, The touchscreen controls of SpaceX's Crew Dragon give astronauts a sci-fi way to fly in space (2020); www.space.com/spacex-crew-dragon-touchscreen-astronaut-thoughts.html [accessed 8 June 2021].
40. M. Panzirsch, H. Singh, T. Krueger, C. Ott, A. Albu-Schäffer, Safe interactions and kinesthetic feedback in high performance earth-to-moon teleoperation, in *Proceedings of the 2020 IEEE Aerospace Conference* (IEEE, 2020).
41. S. Ennis, F. Rometsch, F. Saling, B. Fischer, P. Mittler, L. Ferra, C. Vizzi, Maria Casini Andrea Emanuele, M. Marnat, C. Thevenot, L. Boyer, Astronaut training on-board the International Space Station using a standalone virtual reality headset, in *Proceedings of the International Astronautical Congress* (IAF, 2021).
42. M. J. Schuster, B. Rebele, M. G. Müller, S. G. Brunner, A. Dömel, B. Vodermayer, R. Giubilato, M. Vayugundla, H. Lehner, P. Lehner, F. Steidle, L. Meyer, K. Bussmann, J. Reill, W. Stürzl, I. vonBargen, R. Sakagami, M. Smisek, M. Durner, E. Staudinger, R. Pöhlmann, S. Zhang, C. Braun, E. Dietz, S. Frohmann, S. Schröder, A. Börner, H.-W. Hübers, R. Triebel, B. Foing, A. O. Albu-Schäffer, A. Wedler, The ARCHES moon-analogue demonstration mission: Towards teams of autonomous robots for collaborative scientific sampling in lunar environments, in *Proceedings of the European Lunar Symposium (ELS)* (NASA, 2020).
43. M. A. Vidulich, P. S. Tsang, Absolute magnitude estimation and relative judgement approaches to subjective workload assessment, in *Proceedings of the Human Factors Society Annual Meeting* (SAGE Publications, 1987), pp. 1057–1061.
44. A. Dietrich, C. Ott, A. Albu-Schäffer, An overview of null space projections for redundant, torque-controlled robots. *Int. J. Robot. Res.* **34**, 1385–1400 (2015).
45. S. Stramigioli, *Modeling and IPC Control of Interactive Mechanical Systems—A Coordinate-Free Approach* (Springer, 2001).
46. A. Albu-Schäffer, C. Ott, U. Frese, G. Hirzinger, Cartesian impedance control of redundant robots: Recent results with the DLR-light-weight-arms, in *Proceedings of the 2003 IEEE International Conference on Robotics and Automation* (IEEE, 2003), vol. 3, pp. 3704–3709.
47. M. Panzirsch, T. Hulin, J. Artigas, C. Ott, M. Ferre, Integrating measured force feedback in passive multilateral teleoperation, in *International Conference on Human Haptic Sensing and Touch Enabled Computer Applications* (Springer, 2016), pp. 316–326.
48. R. Balachandran, M. Panzirsch, M. de Stefano, H. Singh, C. Ott, A. Albu-Schäffer, Stabilization of user-defined feedback controllers in teleoperation with passive coupling reference. *IEEE Robot. Autom. Lett.* **6**, 3513–3520 (2021).
49. S. G. Hart, L. E. Staveland, Development of NASA-TLX (Task Load Index): Results of empirical and theoretical research, in *Advances in Psychology* (Elsevier, 1988), vol. 52, pp. 139–183.
50. J. Brooke, SUS: A quick and dirty usability scale, in *Usability Evaluation in Industry*, P. W. Jordan, B. Thomas, B. A. Weerdmeester, I. L. McClelland, Eds. (Taylor & Francis, 1996).
51. COL-RIBRE-SPE-0164: Columbus pressurized payloads interface requirements document (2013). Issue 2A.
52. SSP-50313 display and graphics commonality standard (NASA, 2018). Rev. F.
53. E. Ferreira, A. Pereira, A. Gherghescu, L. Gerdes, L. Hann, T. Krueger, Slim robotics: Robotics in a small team with space requirements, in *Proceedings of the International Symposium on Artificial Intelligence, Robotics and Automation in Space (I-SAIRAS)* (NASA, 2020).
54. T. Krueger, F. van der Hulst, E. Ferreira, K. Wormnes, Emiel den Exter, A. Gherghescu, L. Gerdes, L. Hann, A. Pereira, N. Y. Lii, F. Conti, A newcomer's guide to the challenges of a complex space-to-ground experiment, with lessons from Analog-1, in *Proceedings of the International Symposium on Artificial Intelligence, Robotics and Automation in Space (iSAIRAS)* (NASA, 2020).
55. D. M. Dehn, Assessing the impact of automation on the air traffic controller: The shape questionnaires. *Air Traffic Control Q.* **16**, 127–146 (2008).
56. B. G. Witmer, M. J. Singer, Measuring presence in virtual environments: A presence questionnaire. *Presence* **7**, 225–240 (1998).

Acknowledgments: We thank our colleagues at the European Astronaut Center (EAC) for their work on network communication and training in the Analog-1 experiment, as well as from the ESA G. Visentin and P. Schoonejans for enabling the cooperation with DLR, T. B. Rinnan from European Space Operations Center (ESOC) for work on the questionnaire, and K. Pasay and C. Lombardi for the logistics of the mission. We also thank M. Ferraz, who codeveloped an earlier version of the experiment, and colleagues at DLR who helped with the LWR manipulators and developed software: A. Stemmer, O. Eiberger, M. Heumos, A. Beyer, H. Buchner, R. Burger, and F. Schmidt. **Funding:** Analog-1 is an experiment carried out as part of and funded through the European Space Agency's METERON project. METERON is managed from the Human and Robotics Exploration Directorate. Development by DLR for the space experiment was also partially supported by ESA under funding 4000129321/19/NL/RA/ig-ART-STEP. **Author contributions:** M.P., H.S., and R.B. developed and implemented the TDPA-HD. A.P., H.S., and M.P. integrated the manipulation control framework and implemented the Cartesian impedance controller. M.P., T.H., C.O. (control lead), and A.A.-S. developed and implemented the 6-DoF extension of the TDPA. B.W. and A.P. codeveloped and evaluated the questionnaires. For the ISS experiment: E.d.E. and F.v.d.H. (mechanical lead) mainly worked on the hardware of the ESA rover and manipulator. L.H., L.C., L.G., A.G., and E.F. (software lead) mainly worked on the software and networking. K.W., T.K. (robotics lead), J.G. (co-investigator), and W.C. (principal investigator) mainly worked on the logistics. T.K. managed the engineering team. N.Y.L., A.P., D.L., and A.A.-S. managed the DLR contribution. For the analysis: M.P., H.S., and R.B. analyzed the metrics in the objective data. M.P. and H.S. performed the laboratory experiments. M.P. and B.W. prepared, performed, and evaluated the laboratory user study and analyzed the subjective data of the case study. For the manuscript: M.P., A.P., H.S., and B.W. prepared the manuscript. M.P., A.P., H.S., R.B., C.O., N.Y.L., and T.K. discussed the results, and all authors commented. **Competing interests:** Patent applications (German patent application DE 10 2020 115 294 A1, M.P.) related to this work have been filed. The other authors declare that they have no competing interests. **Data and materials availability:** The data for this study have been deposited in the database zenodo with DOI: 10.5281/zenodo.5898549. All other data needed to evaluate the conclusions in the paper are present in the paper or the Supplementary Materials.

Submitted 30 July 2021
Accepted 23 March 2022
Published 20 April 2022
10.1126/scirobotics.abl6307

Downloaded from https://www.science.org at The Hong Kong University of Science and Technology (Guangzhou) on May 25, 2026

Science Robotics

Exploring planet geology through force-feedback telemanipulation from orbit

Michael Panzirsch, Aaron Pereira, Harsimran Singh, Bernhard Weber, Edmundo Ferreira, Andrei Gherghescu, Lukas Hann, Emiel den Exter, Frank van der Hulst, Levin Gerdes, Leonardo Cencetti, Kjetil Wormnes, Jessica Grenouilleau, William Carey, Ribin Balachandran, Thomas Hulin, Christian Ott, Daniel Leidner, Alin Albu-Schäffer, Neal Y. Lii, and Thomas Krüger

Sci. Robot. **7** (65), eabl6307. DOI: 10.1126/scirobotics.abl6307

View the article online
https://www.science.org/doi/10.1126/scirobotics.abl6307
Permissions
https://www.science.org/help/reprints-and-permissions

Downloaded from https://www.science.org at The Hong Kong University of Science and Technology (Guangzhou) on May 25, 2026

Use of this article is subject to the Terms of service

Science Robotics (ISSN 2470-9476) is published by the American Association for the Advancement of Science. 1200 New York Avenue NW, Washington, DC 20005. The title *Science Robotics* is a registered trademark of AAAS.

Copyright © 2022 The Authors, some rights reserved; exclusive licensee American Association for the Advancement of Science. No claim to original U.S. Government Works